Liquid-State Theory of Structure, Thermodynamics, and Phase Separation in Suspensions of Rod Polymers and Hard Spheres†

Y.-L. Chen and K. S. Schweizer*

Departments of Chemical and Biomolecular Engineering, Materials Science and Engineering, and the Materials Research Laboratory, University of Illinois, Urbana, Illinois 61801

Received: September 2, 2003; In Final Form: December 3, 2003

A new formulation of the polymer reference interaction site model (PRISM) theory for suspensions of hard spheres and rigid rods has been developed. The nonlocal loss of orientational entropy when a rod is near an impenetrable particle is accounted for in a thermodynamically self-consistent manner. In the ideal needle limit, quantitative predictions and qualitative scaling behaviors are determined for the depletion potential, rod insertion chemical potential, intermolecular pair correlations, and fluid−fluid spinodal phase-separation boundaries as a function of rod−particle size-asymmetry and mixture variables. The needle-induced depletion potential of mean force between a pair of particles is in good agreement with exact numerical results and experiments on dilute silica−virus suspensions. Needle-induced clustering of colloidal particles is studied, and the PRISM results are in good agreement with the small amount of available simulation data. The behavior of spinodal boundaries in the extreme size-asymmetry ratio limits is predicted to be qualitatively different, in contrast with that reported from prior approaches based on free volume/scaled particle theory or a density functional approach that finds that a universal description applies. The influence of rod−rod repulsions far from the isotropic−nematic phase transition is found to be minor.

I. Introduction

The complex phase behavior and rheology of polymer−colloid mixtures and their potential application as nano- and biological advanced materials have spurred extensive interest in understanding how to control their physical interactions, structure, properties, and equilibrium and nonequilibrium (gel, glass) state selection.[1−6] Simulations[7−12] and theoretical approaches based on the classic Asakura−Oosawa (AO) model,[13−16] field theory,[17−20] density functional theory (DFT),[21−23] phantom sphere free-volume model (PSFV),[24,25] and integral equation theory[5,6,26−31] have been reported for mixtures of flexible nonadsorbing polymers and spherical particles. The latter are typically model hard spheres, which is the focus of the present paper.

The simplest classical statistical thermodynamic approaches[13−16,24] treat small, flexible polymers (radius of gyration R_g) as phantom spheres of diameter $2R_g$ that do not interact with each other but interact as hard spheres with particles (radius R). Multiple physical aspects are ignored, including (i) polymer−polymer repulsive interactions in good or athermal solvents, (ii) chain connectivity and internal polymer conformational degrees of freedom, and (iii) beyond lowest order in polymer concentration effects. Under good solvent conditions, the original classical theory[13,24] makes qualitatively incorrect predictions for the dependence of fluid−fluid phase-separation boundaries on the size-asymmetry ratio R_g/R.[5,6,24] Several very recent studies have focused on improving this statistical thermodynamic approach[10,11,25] by relaxing simplifications i and/or ii.

The microscopic polymer reference interaction site model (PRISM) theory of thermodynamics, structure, and demixing has recently been generalized to treat polymer−particle suspensions.[28−30] A novel modified Percus−Yevick (mPY) closure approximation for polymer−particle direct correlations captures, in a thermodynamically self-consistent manner, nonlocal entropic repulsions and the loss of conformational entropy associated with polymer segments close to impenetrable particles. Simplifications i−iii are not invoked. No adjustable parameter predictions of PRISM-mPY have been subsequently verified by systematic experimental studies of the phase boundaries,[5,6] colloidal osmotic compressibility,[6,31] and colloidal structure[32,33] of model polymer−particle suspensions as a function of the particle volume fraction ϕ_s, R_g/R, polymer concentration (c_p), and solvent quality (ideal θ versus athermal). The critical importance in many situations of points i and ii, and to a lesser extent point iii, has been demonstrated.

Suspensions of rigid rod macromolecules and spherical particles have been far less studied. Depletion attraction effects are dependent on macromolecular shape and rigidity. Such suspensions are important[34−39] in many biological and surfactant systems where viruses and rodlike micelles often have large persistence lengths and can interact with spherical particles of a diameter that can be greater than, comparable to, or less than the rod length L ($R_g = L/\sqrt{12}$). An additional complexity is the possibility of rod alignment and an isotropic−nematic transition at high enough polymer concentrations. In the absence of particles, Onsager theory predicts that the latter occurs for hard rods of thickness d at $c_p^{NI} = 4.2/L^2d$.[40,41] Almost all prior theoretical and simulation studies of rod−sphere mixtures[8,22,42−46] have avoided this complication by either working at $c_p \ll c_p^{NI}$ and $c_p > c_p^*$ or $c_p < c_p^*$ (where $c_p^* = 3/(4\pi R_g^3)$ is the dilute−semidilute crossover concentration) or employing a noninteracting ideal rod ("needle") model corresponding to $d \to 0$.

Simulations[8] and simplified density functional theory[22] based on modeling a rod as a rigid body characterized by its center of mass and orientation have been applied to determine the phase

† Part of the special issue "Hans C. Andersen Festschrift".

* Corresponding author. E-mail: kschweiz@uiuc.edu.

10.1021/jp036613q CCC: $27.50
Published on Web 02/24/2004

behavior of mixtures of particles (diameter $D = 2R$) and ideal needlelike rods. Stable fluid−fluid coexistence regions for $L/D > 1$ are found. Because the prior theoretical approaches[8,22] for rod polymers avoid approximating them as spheres, the differences between them and PRISM theory are expected to be more subtle than those found for the flexible-coil systems.

The goal of the present paper is to formulate and apply a new PRISM-mPY theory to treat rigid rod−particle suspensions. Our primary focus is the ideal needle limit in order to allow comparison with prior simulations and theory. Whether the nonlocal entropic effects of critical importance for flexible coils are also relevant for rigid rods is a priori not known. For dilute rod−sphere mixtures, our prior PRISM studies based on the local site−site Percus−Yevick closure (PRISM-PY)[44,45,47] for rod−particle direct correlations have been shown to agree quantitatively (perhaps fortuitously) with exact numerical calculations of depletion attractions in the nanoparticle limit ($L/R \to \infty$). However, the rod-induced depletion attraction between particles in the colloid limit ($L/R \to 0$) is strongly underpredicted. Moreover, for all size-asymmetry ratios, the PRISM-PY predictions for the shape of the rod−particle pair correlation function near contact is qualitatively incorrect, as is also true for the flexible-coils case.[27,48] This failure is due to the neglect by the site−site PY closure of nonlocal constraints on the rod orientational entropy when it is close to an impenetrable sphere.

The remainder of the paper is structured as follows. In section II, we briefly review PRISM theory for random coil−sphere mixtures and present a new, more general argument for the inclusion of nonlocal entropic repulsions effects. This provides the basis for an extension to treat rigid rods. Section III presents predictions in the dilute particle limit and makes comparisons with exact results and experiment. Phase separation in ideal needle−particle mixtures is the topic of section IV. The paper concludes in section V with a summary and discussion of future directions. The influence of rod−rod repulsion is briefly addressed in the Appendix.

II. Theory

We begin by briefly reviewing the PRISM-mPY theory for mixtures of particles and flexible coils. A more intuitive derivation of the mPY idea for coil−particle direct correlations is presented, which serves as the foundation for the generalization to rigid rods and other polymer architectures.

A. PRISM Theory for Particle−Coil Mixtures. The microscopic PRISM approach is a generalization of the small-molecule RISM theory of Chandler and Andersen.[49,50] For a binary mixture composed of species of symmetry-equivalent sites, the generalized Ornstein−Zernike, or Chandler−Andersen, matrix integral equations in Fourier space are given by

$$\hat{h}_{ij}(k) = \hat{\omega}_i(k)[\hat{C}_{ij}(k)\,\hat{\omega}_j(k) + \sum_l \hat{C}_{il}(k)\,\rho_l \hat{h}_{lj}(k)] \qquad (1)$$

where $g_{ij}(r) = h_{ij}(r) + 1$, ($C_{ij}(r)$) is the intermolecular site−site pair (direct) correlation function between sites of species i and j, $\hat{\omega}_i(k)$ is the intramolecular structure factor, k denotes the wavevector, and ρ_i is the site number density of mixture species i. For hard spheres, $\hat{\omega}_s(k) = 1$. A field theoretic-like effective Gaussian random walk, or continuum thread, model of a homopolymer chain composed of N segments of statistical segment length σ is adopted,[40] for which

$$\hat{\omega}_p(k) \cong \frac{1}{N^{-1} + \frac{(k\sigma)^2}{12}} \qquad (2)$$

The site−site PY closure[47,49] for mixtures where all interactions are hard-core repulsions is given by

$$\begin{aligned} C_{ij}(r) &= 0 \qquad r > R_{ij} \\ g_{ij}(r) &= 0 \qquad r < R_{ij} \end{aligned} \qquad (3)$$

where R_{ij} is the distance of closest approach between two sites. For ideal thread polymers, $C_{pp}(r) = 0$ for all r, consistent with a vanishing second virial coefficient appropriate to θ-solvent conditions.[51] The local (short-ranged) nature of the PY closure does not account for restrictions on the polymer conformational entropy due to interactions with particles. One manifestation of this is that PRISM-PY theory predicts that the coil−sphere site−site correlation function scales as $g_{ps}(r) \sim (r - R)$ near contact, which is in qualitative disagreement with the known exact behavior of $g_{ps}(r) \sim (r - R)^2$.[19,20] The direction of the error is such that it strongly underestimates the depletion effect (i.e., the tendency for polymer segments to be pushed away from the particle surface for entropic reasons).

A spectacular consequence of the local nature of PRISM-PY theory is that it does not predict fluid−fluid phase separation under athermal solvent conditions,[28,30] in stark disagreement with experiment. Such a problem is analogous to the well-known failure of PY theory for hard-sphere mixtures to predict entropy-driven demixing.[52] Nonlocal direct correlations and the loss of conformational entropy when polymer segments are close to, but not in contact with, a hard sphere must be taken into account.[28,30] It is known from field theoretic studies[20] that the spatial range of the nonlocal disturbance, λ, for the one-polymer and one-particle problem is $\lambda \sim R_g$ in the $R \gg R_g$ "colloid" or "wall" limit and that $\lambda \sim R$ in the $R \ll R_g$ "nanoparticle" limit. In the framework of liquid-state theory, the capture of this physics requires $C_{ps}(r)$ to be nonzero beyond contact ($r > R$).

The mPY closure has been formulated to capture this nonlocality of the polymer−particle direct correlation functions in an average, self-consistent, and predictive manner. A nonlocality function, $F(r)$, is introduced[28−30] as

$$\begin{aligned} C_{ps}(r) &= \int C_{ps}^{PY}(r') \cdot F(|\vec{r} - \vec{r}'|)\, d\vec{r}' \\ \hat{C}_{ps}(k) &= \hat{C}_{ps}^{PY}(k) \cdot \hat{F}(k) \end{aligned} \qquad (4)$$

In hindsight, this form bears some similarities to the nonlocal version of weighted-density functional theory.[53] The PY component of the direct correlation function in eq 4 satisfies the same closure in eq 3. The nonlocality or "smearing" function is normalized such that $\hat{F}(0) = 1$. Further specification was guided by the known physics of the nonlocality length, λ, plus the desire to allow analytic progress to be made in solving the coupled integral equations on the basis of Wiener−Hopf factorization methods. This motivated the specific choice of $F(r) \propto e^{(-r/\lambda)}/r$, or a Lorenztian in Fourier space, parametrized solely by the nonlocality length:[28]

$$\hat{F}(k) = \frac{1}{1 + (k\lambda)^2} \qquad (5)$$

The PY closure is recovered in the $\lambda = 0$ limit. Physically, λ is expected to be a function of all system variables, which for the

present problem are R_g, R, polymer segment density, and particle volume fraction ϕ_s.

In the low polymer-concentration limit, the nonlocality parameter is determined via a thermodynamic self-consistency procedure. The compressibility route and the free-energy route calculations of the chemical potential for inserting a single polymer into the particle fluid are given by[28,50]

$$N\beta\delta\mu_p|_{\rho_p=0} = -\int_0^{\rho_s} N\hat{C}_{ps}(k=0;\rho_s')\,d\rho s' \quad \text{(compressibility)} \quad (6)$$

$$N\beta\delta\mu_p|_{\rho_p=0} = \frac{3\phi_s N}{g'_{ps}(R)|_{L/D\to 0}}\int_0^1 \zeta^2 g'^{(\zeta)}_{ps}(\zeta R)\,d\zeta + 2\pi N\rho_s{}^2 D^3\int_0^1 \zeta^2 \frac{\partial}{\partial\rho_p} g^{(\zeta)}_{ss}(\zeta D)\,d\zeta \quad \text{(free energy)} \quad (7)$$

Here, ζ is a charging parameter that "grows" the particle from a point to its full diameter, and the $g_{ij}^{(\zeta)}$'s are evaluated for particles of diameter ζD. The nonlocality parameter is determined by requiring eqs 6 and 7 to yield identical results. Equations 1−7 plus the thermodynamic consistency constraint are thus a closed set of four equations.

To go beyond the dilute polymer limit, the effect of polymer−polymer correlations on the nonlocality effect must be taken into account. This has been achieved using the classic "blob scaling" idea from polymer physics,[28,54] the details of which are not important for our present work because rod−rod interactions are absent in the ideal needle model. We note that in the dilute colloid and $R \gg R_g$ limit, for all polymer concentrations, λ is predicted to be equal to the density−density correlation length of the pure polymer fluid, ξ_ρ, in agreement with field theory and other physical arguments.[19,20,54] In the low polymer-concentration limit, ξ_ρ reduces to the single-polymer correlation length, $\xi_c = R_g/2^{1/2}$ based on eq 2.

It is the motivation for the specific choice in eq 5 that we revisit here. The Lorentzian form previously adopted for analytic convenience is actually identical to the thread PRISM collective density−density fluctuation structure factor, $\hat{S}(k)$, of the pure polymer system:[55,56]

$$\hat{S}(k) = \frac{\hat{S}(0)}{1+(k\xi_\rho)^2} \to \hat{\omega}(k) = N(1+(k\xi_c)^2)^{-1}, \quad c_p \to 0 \quad (8)$$

Hence, the spatial form of $F(r)$ is identical to that of the collective polymer density fluctuations or single-chain density correlations in the dilute limit. This recognition provides additional physical interpretation of the mPY idea. That is, in addition to the "direct" through-space interaction between a polymer segment and a particle, there are "indirect" pathways mediated by polymer density correlations or connectivity correlations in the dilute polymer limit. Figure 1 schematically illustrates this idea. On the basis of this insight, generalization of the mPY closure to other polymer architectures follows naturally.

B. Nonlocal Entropy Effects for Rod Polymers. We consider a continuum needle model of a polymer rod of length L, for which the intramolecular structure factor (normalized to unity at $k = 0$) is given by

$$\tilde{\omega}_p(k) = \lim_{N\to\infty}\frac{1}{N}\hat{\omega}_p(k) = 2\int_0^1 (1-t)\frac{\sin(tkL)}{tkL}\,dt \quad (9)$$

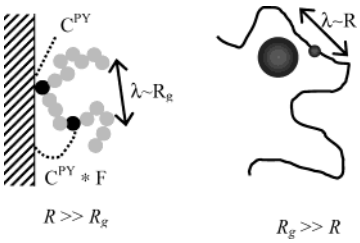

Figure 1. Schematic illustration of the nonlocal entropic effect for one particle and one random-coil polymer. In the $R_g \ll R$ extreme colloid limit, the particle is wall-like, and perturbations of the conformation entropy extend to a distance of $\lambda \sim R_g$. In the $R \ll R_g$ nanoparticle limit, the particle perturbs the polymer conformation on the scale of $\lambda \sim R$.

where N is the number of sites per rod, which is taken to infinity for the continuous needle in such a manner that the physical length (L) is finite. The corresponding PRISM integral equations are rewritten in terms of this "intrinsic" single-needle structure factor and appropriately rescaled direct correlation functions, as discussed in detail elsewhere.[51] Although the infinitely thin needles can pass through each other, they cannot pass through the particle. At the site−site level, eqs 1, 3, and 4 again apply. In the $\lambda = 0$ PY limit, we have previously shown[44] that the needle−sphere pair correlations near contact behave as $g_{ps}(r) \sim (r-R)^{1/2}$, which qualitatively disagrees with the known exact behavior[20] of $g_{ps}(r) \sim (r-R)$. The depletion effect in the colloid limit is again greatly underpredicted at short needle−sphere separations.

Following the arguments of section IIA, the nonlocality function appropriate for the problem of a single needle in a sphere fluid is

$$\hat{F}(k) = 2\int_0^1 (1-t)\frac{\sin(tk\lambda)}{tk\lambda}\,dt \quad (10)$$

where λ is a function of L/R and ϕ_s. In the dilute sphere limit, $\lambda = L$ rigorously when $L \ll R$, and $\lambda \sim R$ when $R \ll L$ follows from enforcing thermodynamic self-consistency in the same manner as discussed in section IIIA. In this "double-dilute" limit, the needle insertion chemical potential carries the same information as the needle−particle cross second virial coefficient.

C. Depletion Potential and Thermodynamics. In the infinite dilution limit, the polymer-induced depletion attraction between two spheres can be measured, and the potential of mean force (PMF) is given by $\beta U_{ss}(r) \equiv -\ln[g_{ss}(r)]$. For mixtures containing dilute spheres and polymers, the sphere−sphere pair correlation function is $g_{ss}(r) + 1 = \rho_p W_{ss}(r)$ for $r > R_{ss}$, where[48]

$$\rho_p W_{ss}(r) = FT^{-1}\{\rho_p \hat{C}_{ps}(k)^2 \hat{S}_{pp}(k)\} \quad (11)$$

In the dilute polymer concentration limit, $\beta U_{ss}(r) \approx -\rho_p W_{ss}(r)$.

The insertion chemical potential of adding one needle to a sphere fluid follows from eq 6. Prior studies have also employed an expression from scaled particle theory,[8,57] which is calculated from the available free-volume fraction $\alpha = \exp(-\beta\,\delta\mu_p)$ for inserting a needle into a hard-sphere fluid:

$$\beta\delta\mu_p|_{\rho_p=0} = -\ln\alpha = -\ln(1-\phi_s) + \frac{3}{2}\frac{L}{D}\frac{\phi_s}{1-\phi_s} \quad (12)$$

The prior lowest order in polymer concentration analyses of the phase behavior of needle−sphere mixtures has employed eq 12.[8,22,57]

We have previously carried out the rigorous lowest order in polymer concentration perturbative analysis of the fluid−fluid

spinodal condition within the PRISM framework, which is referred to as O(c_p) PRISM.[51] The dimensionless polymer concentration along the spinodal is given by[51]

$$\frac{c_p^+}{c_p^*} = \frac{V_p}{-2B_{2,pp} + \rho_s \hat{S}_{HS} \Delta\hat{C}_{ss}} = \frac{V_p}{\tilde{C}^0_{pp} + \rho_s \hat{S}_{HS}(\Delta\tilde{C}_{ss} + \tilde{C}^0_{ps})^2} \quad (13)$$

where $V_p \equiv 4\pi R_g^3/3$ is the polymer volume, $\hat{S}_{HS} = \hat{S}_{HS}(0)$ is the hard-sphere dimensionless compressibility, $B_{2,pp}$ is the polymer second virial coefficient, $\tilde{C}^0_{pp} = \lim_{c_p\to 0}\hat{C}_{pp}(0)N^2$, $\tilde{C}^0_{ps} = \lim_{c_p\to 0}\tilde{C}_{ps}(0)N$, and $\Delta\hat{C}_{ss} = \lim_{c_p\to 0}[(\hat{C}_{ss}(0) - \hat{C}_{HS}(0))/c_p]$ is the lowest-order correction of the sphere−sphere direct correlation function due to adding polymers. In literally ideal polymer systems $\tilde{C}^0_{pp}$ is zero, and the competition between the direct needle−particle correlation, $\tilde{C}^0_{ps}$, and needle-induced changes of particle structure, $\Delta\hat{C}_{ss}$, can lead to complex and nonclassical phase behavior, as shown in prior work on coil−particle mixtures.[6,51] The perturbative approach has been found to capture all of the novel trends predicted by the full nonperturbative versions of PRISM-mPY theory for fluid−fluid spinodal boundaries.[6,22,24,51] We focus on the lowest-order spinodals for both computational simplicity reasons and because prior free-volume and DFT free-energy-based studies[22] have worked at this level.

III. Dilute Particle Limit

In this section, we consider the elementary depletion problem of one or two spheres dissolved in an ideal needle solution. Results are compared with exact numerical evaluations and recent experimental measurements of the depletion potential.

A. Nonlocality Length and Needle−Particle Correlations. Thermodynamic consistency can be exactly satisfied by equating eqs 6 and 7 to determine λ as a function of $^L/_R$ and ϕ_s, but it is a numerically intensive trial-and-error computation. On the basis of prior coil−particle mixture studies,[28−30] the simple Padé interpolation equation $\lambda^{-1} = \lambda_0^{-1} + \lambda_\infty^{-1}$ has been shown to work well; the subscripts 0 and ∞ denote the extreme colloid ($^L/_R \ll 1$) and nanoparticle ($^L/_R \gg 1$) limits, respectively. We adopt this approach here.

Consider first the doubly infinite dilute limit of one needle and one or two particles. When $^L/_R \to 0$, $\lambda_0 \to L$ as the needle length becomes the unique characteristic length scale for orientational entropy loss. In the opposite limit ($^L/_R \to \infty$), the particle size controls the needle orientational entropy loss, and one expects $\lambda_\infty \propto R$. Quantitatively, we find $\lambda_\infty = 1.12R$, which can be compared with the analogous result[28] for a flexible random coil of $\lambda_\infty = 2R/(1+\sqrt{5}) \approx 0.6R$. Using the $\lambda^{-1} = L^{-1} + (1.12R)^{-1}$ interpolation equation in conjunction with eqs 6 and 7, we find that thermodynamic consistency is satisfied to within ∼13% over the entire range of $^L/_R$ (inset of Figure 2), a level of accuracy very similar to what was found for random coil polymers.[28]

The main panel of Figure 2 shows examples of the needle−particle pair correlation functions. In contrast to the prior PY-based study,[45] accounting for nonlocal entropy loss yields a $g_{ps}(r)$ that properly increases in a linear manner near contact. The scaling of the separation distance by the nonlocality length demonstrates that the local depletion hole is quantitatively controlled by λ over a wide range of $^L/_R$ ratios. At larger separations, the curves splay apart because the length scale for achieving random packing is controlled by the rod length or, equivalently, the correlation hole length scale.

B. Depletion Potential and Comparison with Exact Results and Experiment. For the system of one needle and two particles, PRISM-mPY predictions of the potential of mean force (PMF) between the particles are shown in Figure 3 in a scaled format where $W_{ss}(h) = U_{ss}(h)/(kTc_pL^2R)$ and $h = r - 2R$ is the separation between the particle surfaces. The results are compared with the exact numerical data of Yaman, Jeppesen, and Marques[46] (YJM) for a needle that is defined only by its length, center of mass, and Euler angle. In the colloid limit, PRISM-mPY predictions for the depletion attraction strength at contact ($W_{ss}(h = 0)$) are in quantitative agreement with the exact results. This represents a substantial improvement over prior PY-based predictions that were a factor of ∼4 too small. However, PRISM-mPY predicts a faster decay of the depletion potential with interparticle distance than the exact behavior.

In the nanoparticle limit, the inset of Figure 3 shows that PRISM-mPY predicts the correct qualitative power law decay of the maximum depletion strength, $W_{ss}(0) \sim {}^R/_L$. However, it is larger than the exact or prior PY-based results by a nearly constant factor of less than 2. Figure 3 also shows that deviations

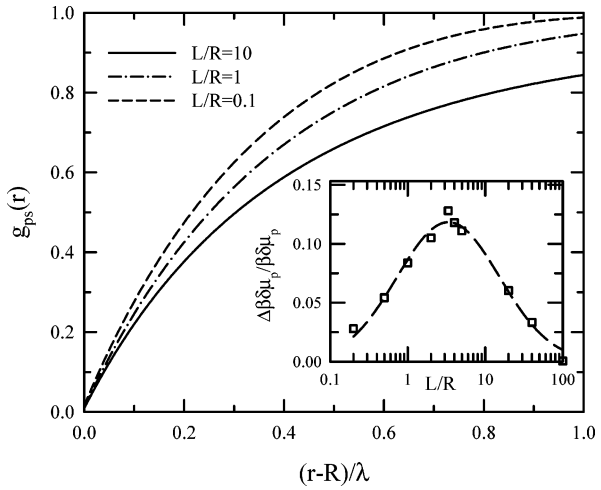

Figure 2. Needle−sphere site−site pair correlation function for $^L/_R = 10$, 1, and 0.1 as a function of reduced separation. The nonlocality lengths in units of L are $\lambda = 0.1$, 0.53, and 0.918, respectively. The inset shows the difference in needle-insertion chemical potential as computed from eqs 5 and 6 divided by the corresponding average of the two thermodynamic integration routes.

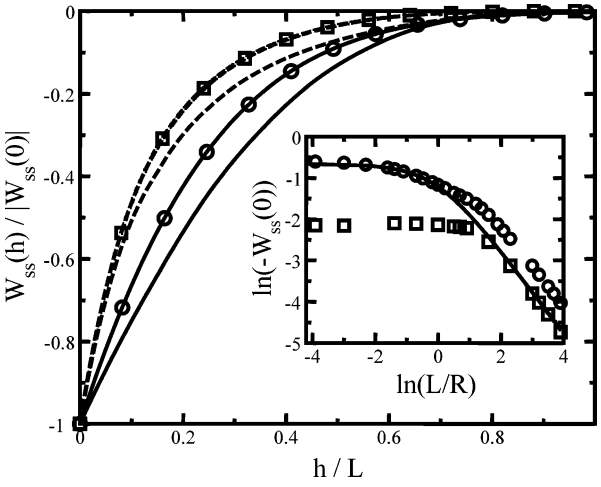

Figure 3. Normalized (to the $h = 0$ contact value) potential of mean force between two particles due to a single rod as a function of reduced surface−surface separation for $^L/_R = 5$ (solid lines) and 0.5 (dashed lines). The exact numerical integration[46] and PRISM-mPY (lines with symbols) results are shown. The inset shows the potential at contact determined from exact numerical integration (solid line), PRISM-mPY (circles), and PRISM-PY (squares).

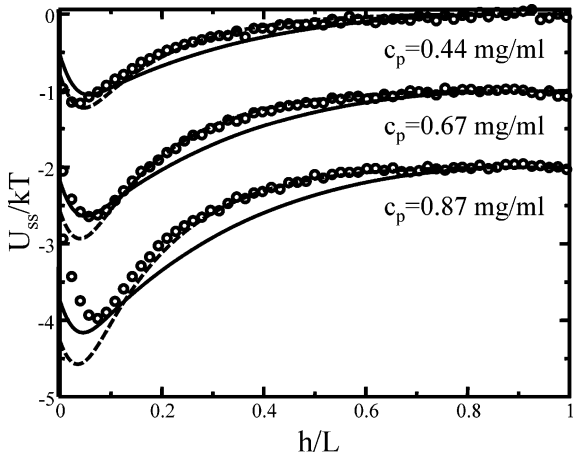

Figure 4. Depletion potential (circles) between two silica particles induced by a dilute solution of the fd virus as measured in ref 58. System parameters are $L = 880$ nm, $D = 1$ μm ($^{L}/_{R} = 1.75$), and $c_p = 0.44$, 0.67, 0.87 mg/mL with the baseline of the potential shifted vertically by 1 as c_p increases. Experimental measurements are compared to numerically exact integration[46] (solid lines) and PRISM-mPY (dashed lines) results.

between the theory and exact results for the shape of the depletion potential are qualitatively identical to that found in the colloid regime.

Recent optical tweezer experiments[58] have measured the depletion attraction potential between dilute silica spheres ($^{L}/_{R} \approx 1.75$) induced by the needlelike fd virus (aspect ratio, $^{L}/_{d} \approx 140$) at relatively dilute polymer concentrations of $c_p/c_p^{NI} = 0.044$, 0.067, and 0.087, far from the isotropic−nematic phase transition. To compare the experiment quantitatively to the exact numerical solution[46] and PRISM-mPY results, the theoretical results must be numerically smeared by convolution with a Gaussian kernel with a half-width of 30 nm ($^{\sigma}/_{L} = 0.034$).[58] Results are shown in Figure 4. The theoretical depletion potentials scale linearly with needle density. As noted previously,[58] the numerically exact solution is in good agreement with the experimental depletion attraction strength, but it predicts a slightly slower decay than observed. The PRISM-mPY prediction at the lowest needle concentration agrees quantitatively with experiments for both the depletion strength and range but overpredicts the strength of the depletion attraction as the needle concentration increases. Because the fd virus is charged, even though the Debye−Huckel screening length is relatively short the presence of residual inter-rod Coulomb repulsions could be the origin of an apparently weaker-than-linear increase of the experimental depletion attraction strength with polymer concentration.

Overall, the quality of agreement between PRISM theory and experiment is quite good, although perhaps partially fortuitous because there are several differences between the theoretical model and the experimental system. The fd virus is not perfectly rigid,[58,59] the concentrations are not infinitely dilute, and the interactions are not perfectly hard core. An alternative recent theoretical approach that uses the flexibility of the fd virus as a fitting parameter has been found to be in even better agreement with the experiments.[59]

IV. Needle−Particle Mixtures

We now consider mixtures of ideal needles and nondilute hard spheres. The dependence of λ on particle volume fraction has been numerically determined using eqs 6 and 7 over the range from $\phi_s = 0-0.55$. The Padé method is again employed to interpolate the numerical results, which are very well reproduced by the analytic form

$$\lambda^{-1} = L^{-1} + ((1 - \phi_s^2)1.12R)^{-1} \tag{14}$$

Equation 14 satisfies thermodynamic consistency to within 15% (or much less) over the entire range of ϕ_s. The qualitative trends with particle volume fraction are the same as those found previously for coil−particle mixtures.[28] As more particles are added, the nonlocal correlation length is monotonically reduced. Physically, this is due to increasing local needle−particle contacts and the interference of depletion layers between particles. In the extreme colloid limit, the nonlocality length is independent of particle volume fraction as expected on the basis of simple geometric considerations. In the nanoparticle limit, $\lambda \approx (1 - \phi_s^2)(1.12R)$, which differs significantly from the random coil−sphere mixture result[28,30] of $\lambda \approx [(2\ R)(1 - \phi_s)]/[(\sqrt{5} + 1)(1 + 2\phi_s)]$. As ϕ_s increases, λ in the needle−nanoparticle system decreases much more slowly ($\lambda = 0.84\ R$ for $\phi_s = 0.5$) than in the coil−sphere system ($\lambda = 0.15R$ for $\phi_s = 0.5$). This implies that the nonlocal entropic constraints due to the presence of nanoparticles are more severe for flexible coils presumably because they are more globular objects and tend to have more contacts with nanoparticles than a rigid rod does.

A. Rod Insertion Chemical Potential. The insertion chemical potential, $\beta\delta\mu_p(^{L}/_{R}, \phi_s)$, for adding a single needle to the hard-sphere fluid is a property of fundamental interest. PRISM-mPY theory predicts that the integrated strength ($k = 0$ value) of the needle−particle direct correlation function scales as $\tilde{C}_{ps}^{0} \sim LR^2$ in the nanoparticle limit and as $\sim R^3$ in the colloid limit at all particle volume fractions. This scaling is consistent with the exact behavior for a single needle and particle or the corresponding cross second virial coefficient, as follows from elementary geometric considerations.

PRISM-mPY calculations of the insertion chemical potential based on eq 6 are shown in Figure 5A, along with the scaled particle theory (SPT) results.[8] To establish the role of nonlocal entropic repulsion effects, the analogous PRISM-PY results ($\lambda = 0$) are also shown. In the $^{L}/_{R} \to 0$ colloid regime, SPT, PRISM-mPY, and PRISM-PY are (trivially) in quantitative agreement to zeroth order in $^{L}/_{D}$ because $\beta\delta\mu_p = -\ln(1 - \phi_s) + O(^{L}/_{D})$. In the nanoparticle regime, all three approaches predict that $\beta\delta\mu_p \sim {}^{L}/_{D}$. Curiously, the SPT and PRISM-PY results are in essentially quantitative agreement, consistent with the findings in Figure 5A. This may suggest, but does not prove, that SPT (which is a PY-type approximation within a rigid body treatment of the rod) and PRISM-PY both ignore aspects of the nonlocal entropic repulsion effect. The PRISM-mPY chemical potentials are systematically higher, which we identify as a consequence of the nonlocal entropic repulsion effect.

Derivatives of the insertion chemical potential play a critical role in the phase-separation predictions of the free-volume theory, which is equivalent to the simplified DFT.[8,22] As seen from eq 12, SPT predicts that $\beta\delta\mu_p$ scales linearly with $^{L}/_{D}$ for all ϕ_s and size-asymmetry ratios, $\partial(\beta\delta\mu_p)/\partial(^{L}/_{D}) = (^{3}/_{2})\phi_s/(1 - \phi_s)$. A priori, we cannot think of a compelling reason that the insertion chemical potential should be a linear function of $^{L}/_{D}$ for all size-asymmetry ratios, and this behavior may be closely related to the PY-like basis of SPT. In contrast, Figure 5B shows that PRISM-mPY theory predicts that $\beta\delta\mu_p$ scales linearly with $^{L}/_{D}$ at a fixed ϕ_s only in the extreme limits of $^{L}/_{D} \to \infty$ and $^{L}/_{D} \to 0$, with different prefactors in each limit. As shown below, this is an important difference with major consequences for phase-separation boundaries.

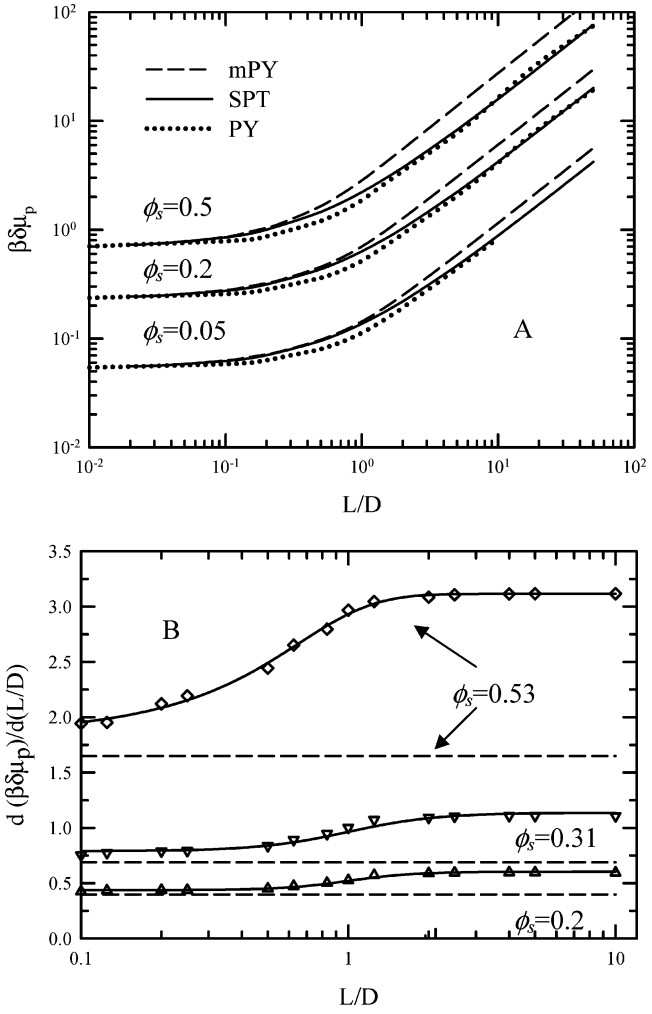

Figure 5. (A) Dimensionless needle-insertion chemical potential as predicted by SPT, PRISM-mPY, and PRISM-PY calculated using the compressibility route (eq 5) as a function of $^{L}/_{D}$ at three particle volume fractions. (B) Derivative of the insertion chemical potential with respect to $^{L}/_{D}$ at three particle volume fractions for SPT (horizontal dashed lines) and PRISM-mPY (points with smooth interpolation curves).

B. Fluid−Fluid Phase Separation. Given the insertion chemical potential and the pure hard-sphere compressibility,[60,61] $\hat{S}_{HS} = (1 - \phi_s)^4/(1 + 2\phi_s)^2$, the perturbative O($c_p$) spinodals are[24,51]

$$\frac{c_p^{+}}{c_p^{*}} = (\phi_s \hat{S}_{HS})^{-1}\left(\frac{R_g}{R}\right)^3 \alpha\left(\frac{\partial^2\alpha}{\partial\phi_s^{\,2}}\right)^{-1} \qquad (15)$$

where c_p^{+} is the needle concentration at the spinodal as discussed in detail previously.[51] Equation 15 is strictly equivalent to eq 13 for ideal polymers when the following Maxwell's relation[62] is employed:

$$\frac{1}{\alpha}\left(\frac{\partial^2\alpha}{\partial\phi_s^{\,2}}\right) = \left(\frac{\pi}{6}D^3\right)^2(\Delta\hat{C}_{ss} + \tilde{C}_{ps}^{0\ 2}) \qquad (16)$$

The quantity $\kappa = \alpha^{-1}(\partial^2\alpha/\partial\phi_s^2) \propto [(\partial^2\beta\delta\mu_p/\partial\phi_s^2) - (\partial\beta\delta\mu_p/\partial\phi_s)^2]$ defines a free-volume fraction curvature, which is of central importance in determining the spinodal boundaries. When viewed as the difference in derivative(s) of the chemical potential, it also would seem to be a rather subtle quantity to compute. Within PRISM theory, eq 13 shows that the predicted phase-separation behavior is very sensitive to the competition between needle−particle direct correlations ($\tilde{C}_{ps}^{0}$) and the needle-induced change in the particle−particle direct correlations ($\Delta\tilde{C}_{ss}$).

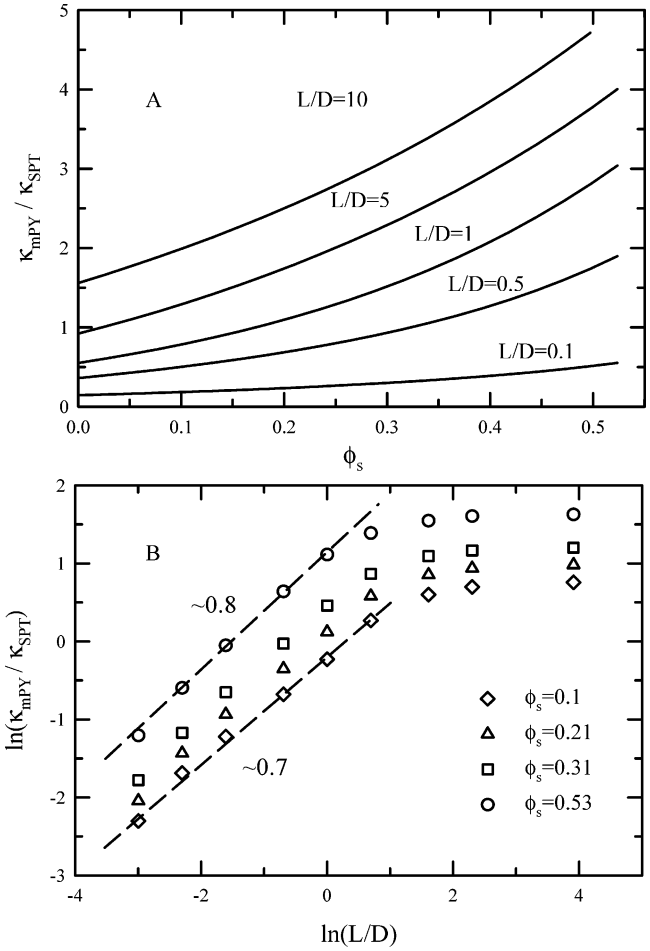

Figure 6. (A) Ratio of the PRISM-mPY and SPT curvatures of the insertion chemical potential as a function of ϕ_s at various $^{L}/_{D}$ values. (B) Ratio of the PRISM-mPY and SPT curvatures of the insertion chemical potential as a function of $^{L}/_{D}$ at various ϕ_s values. Effective power law behavior and the corresponding exponents in the $^{L}/_{D} < 1$ regime are indicated.

Parts A and B of Figure 6 quantify the significant differences between the PRISM-mPY and SPT predictions for the free-volume fraction curvature. There are three major trends. (i) PRISM predicts higher curvature than SPT for large $^{L}/_{D}$ and/or high ϕ_s, which will result in spinodal phase separation at lower values of rod concentration (eq 13). (ii) PRISM theory curvatures are in qualitative agreement with SPT in the nanoparticle regime in the sense that the curvature ratio becomes asymmetry-ratio-independent at large $^{L}/_{D}$ (Figure 6B). (iii) In the intermediate ($L \approx D$) and extreme colloidal ($L \ll D$) regime, the curvature ratio empirically follows a power law $(^{L}/_{D})^{\nu}$ with $\nu \approx 0.7-0.8$. All of these differences are consistent with the results of Figure 5B and are also present when SPT is compared with the results of PRISM-PY theory (not shown). Hence, these differences are not qualitatively due to the nonlocal repulsion effect. Rather, they appear to arise from fundamental differences between the approximations (closures) inherent to SPT for rigid rods and the interaction-site-based PRISM approach.

The curvature differences between PRISM-mPY theory and SPT hold major consequences for the qualitative behavior of the spinodals boundaries shown in Figure 7.

The DFT[22] and free-volume[8] approaches make identical spinodal predictions based on SPT input for the needle-insertion

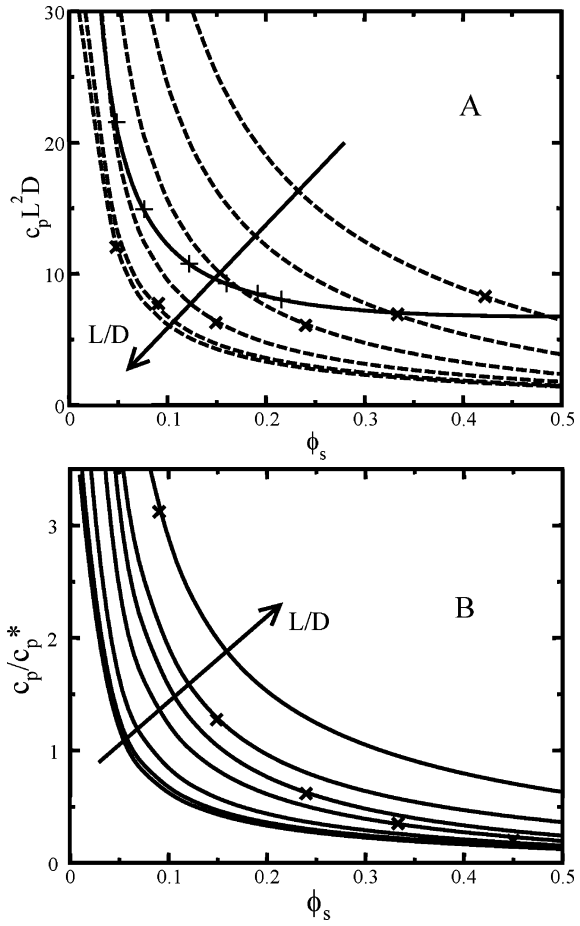

Figure 7. (A) O(c_p) spinodal boundary predictions of the ideal needle−sphere mixture with L^2D as the nondimensionalizing volume for polymer concentration for PRISM-mPY (dashed lines) and DFT (single solid line). PRISM results (bottom to top) are shown for $^L/_D = 10$, 5, 2, 1, 0.5, and 0.25. PRISM (×) and DFT (+) critical points are also shown, with ϕ_s^{crit} decreasing as $^L/_D$ increases. (B) PRISM-mPY predictions of the O(c_p) spinodal boundary with the dilute−semidilute crossover needle concentration as the nondimensionalizing factor for $^L/_D = 4$, 2, 1, 0.5, 0.2, 0.1, and 0.05 (top to bottom). The crosses indicate the critical points.

chemical potential. They predict that the spinodal boundaries are independent of $^L/_D$ when expressed in reduced units of $c_p^+L^2D$:[22]

$$c_p^+L^2D = \frac{8(1+2\phi_s)^2}{3\pi\phi_s} \tag{17}$$

We do not have an intuitive understanding of why this reducing variable should result in a universal curve, and to the best of our knowledge, no such argument has been given in the literature. In strong contrast, Figure 7A shows in these reduced units that the PRISM-mPY spinodals shift to lower values of $c_p^+L^2D$ at fixed ϕ_s as $^L/_D$ increases, with a collapse onto a universal curve only in the extreme nanoparticle limit. An additional significant difference between the two theories involves the shape of the spinodal curve. The DFT/SPT spinodals are exceptionally flat at high particle volume fractions, in strong contrast to the PRISM results.

Figure 7B presents the same theoretical spinodals but in the different scaled polymer concentration representation of c_p/c_p^*. The latter is the classic way of plotting phase diagrams for polymer−colloid suspensions because the dilute−semidilute concentration signals the point when macromolecules thought of as spherical objects begin to interact or overlap. As seen from Figure 7B, both the PRISM and DFT spinodals shift to higher c_p^+/c_p^* at fixed ϕ_s as the size-asymmetry ratio $^L/_D$ increases. Interestingly, this direction of shifting is precisely the opposite of what all theories for ideal random coils predict,[6,24,51] thereby demonstrating the importance of macromolecular architecture and rigidity. The PRISM spinodals collapse in the colloid limit, and DFT predicts that $c_p^+/c_p^* \propto {}^L/_D$. Hence, even though the $\beta\delta\mu_p$ predictions of SPT and PRISM are in near-quantitative agreement in the colloid limit (Figure 5A), vastly different qualitative phase behavior emerges because of the differences in the curvatures of the insertion chemical potentials (Figure 6). Perturbative spinodals determined using the PRISM-PY theory (not shown) follow the same qualitative behavior as those of PRISM-mPY theory. The PY closure-based spinodals lie at quantitatively larger values of reduced polymer concentration, as expected from the absence of nonlocal needle−sphere repulsion.

It is instructive to contrast the present needle−sphere behavior with its ideal random coil analogue, which has been numerically and analytically analyzed in great detail within both the PRISM[28,51] and free-volume/DFT/SPT frameworks.[23,24] For ideal coils, we have recently shown[6,51] that the direction of shifting of spinodals with a size-asymmetry ratio, R_g/R, is in the same direction for both theories in the colloid limit. In the c_p/c_p^* representation, the spinodals shift downward proportional to $(R/R_g)^3$ in the free-volume/SPT approach and proportional to (R/R_g) in PRISM theory for either the PY or mPY closure. The different scaling with R/R_g arises from the unrealistic representation of large polymers ($R_g > R$) as impenetrable spheres by the free-volume approach. In the colloidal regime ($R_g \ll R$), which is most relevant to the present issue of differences between the two theories for rods, all theories make qualitatively identical predictions[8,22] for the spinodal boundaries that saturate in the c_p/c_p^* representation as $R_g/R \rightarrow 0$. This agreement in the ultrasmall polymer limit has been understood as a natural consequence of the qualitative irrelevance of polymer internal (conformational) degrees of freedom when particles are so huge that they cannot penetrate the domain of the macromolecule.[30] The latter argument would seem to be generic, and we see no reason that it would not apply to the rod case. Hence, the behavior predicted by PRISM theory for rods in the extreme colloid limit seems intuitive to us. If our analysis of the situation is correct, then it points to subtle errors in the SPT calculation of the first and second derivatives of the needle-insertion chemical potential for very small rods.

We have addressed the accuracy of the lowest-order perturbative calculations of spinodals by performing a limited, but representative, numerical study based on full, nonperturbative PRISM theory. We refrain from presenting more figures and summarize only what has been found. The qualitative trend of increased fluid−fluid miscibility in the representation of ϕ_s versus c_p/c_p^* as $^L/_D$ increases is preserved. The O(c_p) spinodals are at lower needle concentrations than the full spinodals, as found in prior studies of ideal coil mixtures,[51] but for all, particle volume fractions are less than a factor of 2 lower over the range from $^L/_D = 0.5-5$. For example, at $^L/_D = 0.5$, $c_{p,o(c_p)}^+/c_{p,full}^+ \approx 0.5$ for $\phi_s = 0.05-0.5$. At $^L/_D = 5$, $c_{p,o(c_p)}^+/c_{p,full}^+ \approx 0.75-0.9$ over $\phi_s = 0.05-0.5$, and the ratio grows as ϕ_s increases and c_p^+ decreases (approaching the perturbative limit).

Finally, carefully designed computer simulations that penetrate well into the $L < D$ regime are required to decide definitely what the correct shifting of fluid−fluid phase separation boundaries is as a function of $^L/_D$. To avoid depletion-

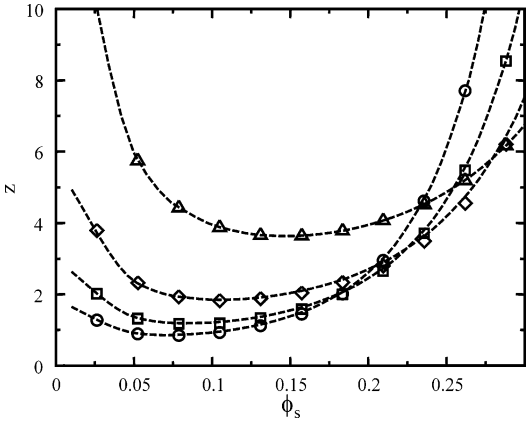

Figure 8. PRISM-mPY fugacity at the spinodal phase boundary of the ideal needle−particle mixture for $^{L}/_{D} = 5$ (circles), 4 (squares), 3 (diamonds), and 2 (triangles). The curves are cubic splines drawn to guide the eye.

TABLE 1: Critical Polymer Fugacities and Particle Volume Fractions of the Ideal Needle−Particle Mixture[a]

	c_p^{crit}/c_p*	z^{crit}				ϕ_s^{crit}			
$^{L}/_{D}$	mPY	mPY	PY	SPT	GCMC	mPY	PY	SPT	GCMC
5	4.04	0.81	1.59	1.18	1.4	0.084	0.089	0.073	0.11−0.17
4	3.18	1.16	2.39	1.63	1.8	0.0925	0.099	0.084	0.12−0.17
3	2.06	1.83	4.30	2.48	2.6	0.116	0.136	0.099	0.11−0.17
2	1.29	3.52	9.51	4.63	4.9	0.153	0.168	0.120	0.11−0.19

[a] All theoretical results are based on the lowest order in needle concentration approach, and the simulation (GCMC) results are exact.

induced particle crystallization when $L < D$, a clever trick will be required, for example, using polydisperse colloids that frustrate crystallization but modify the fluid−fluid phase-separation process only slightly. To our knowledge, such simulations do not exist. However, simulations for $^{L}/_{D} > 2$ are available, which we now compare to.

C. Fugacity Representation and Critical Points. Bolhius and Frenkel have employed grand canonical Monte Carlo (GCMC) simulations[8] to study the phase behavior of ideal needle−particle mixtures for $^{L}/_{D} \geq 2$. Their phase diagrams were presented in terms of the fugacity $z = c_p D^3 \exp(\beta\delta\mu_p)$, not needle concentration. We have converted our PRISM spinodal boundary results into the fugacity representation as shown in Figure 8. Because the GCMC simulation determines the fluid−fluid binodal coexistence curves, our spinodal predictions can be quantitatively compared with simulation only at the critical point. The critical particle volume fraction and fugacity results of PRISM-mPY, PRISM-PY, SPT, and GCMC are tabulated in Table 1. For the $^{L}/_{D} \geq 2$ cases studied by simulation, the PRISM-mPY fugacity is systematically smaller than the exact results, suggesting an overestimation of depletion attraction effects. This is consistent with the overestimation of depletion potential in the dilute, small-particle regime (Figure 3 inset). However, the $^{L}/_{D}$ dependence of the PRISM critical fugacity is in close accord with the simulations. The predicted decrease of the critical volume fraction with increasing $^{L}/_{D}$ and its absolute magnitude is also consistent with the simulations to within the considerable uncertainties of the latter.

As expected, PRISM-PY theory predicts larger critical fugacities than its mPY analogue because of its neglect of nonlocal entropic repulsion effects. The deviations decrease monotonically with increasing $^{L}/_{D}$. The latter trend results in a $^{L}/_{D}$ dependence for PRISM-PY that is significantly stronger than for PRISM-mPY or the simulations. Moreover, the PRISM-PY overprediction of the critical fugacity as $^{L}/_{D}$ decreases is

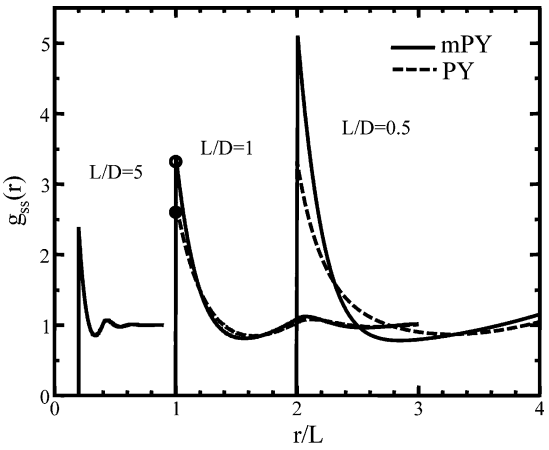

Figure 9. Particle−particle pair correlation function as a function of separation reduced by the needle length for $^{L}/_{D} = 5$, 1, and 0.5, $\phi_s = 0.3$, and $c_p L^2 D = 4.6$. PRISM-PY (dashed lines) and PRISM-mPY (solid lines) results are shown. The Monte Carlo simulation (empty circle) and DFT (solid circle) results for the contact value of the $^{L}/_{D} = 1$ system[22] are also shown.

consistent with the results in Figure 3. The SPT calculations of the critical fugacity agree quite well with the simulation and are systematically smaller (larger) than GCMC (PRISM-mPY) results. The PRISM-mPY, PRISM-PY, and SPT predictions of the critical volume fraction all agree with the simulations within uncertainties. However, SPT predicts that $\phi_s^{crit} \rightarrow 0.25$ as $^{L}/_{D} \rightarrow 0$, whereas over the range of small $^{L}/_{D}$ studied PRISM-mPY yields a ϕ_s^{crit} that increases with decreasing $^{L}/_{D}$.

D. Depletion-Induced Particle Clustering. Differences between PRISM-mPY and PRISM-PY for the particle−particle pair correlation function have also been examined under conditions relevant to the GCMC simulation.[22] Results are shown in Figure 9 at a volume fraction of 0.3 and three values of $^{L}/_{D}$. For the $^{L}/_{D} = 1$ crossover case, the contact values are $g_{ss}(r = D) \approx 3.3$ (simulation), $g_{ss}(r = D) \approx 2.6$ (DFT), $g_{ss}(r = D) \approx 2.75$ (PRISM-PY), and $g_{ss}(r = D) \approx 3.4$ (PRISM-mPY). PRISM-mPY is in excellent agreement with the simulation. DFT and PRISM-PY theory clearly underestimate the depletion-driven local clustering of particles. PRISM calculations for $^{L}/_{D} = 0.5$ and 5 show that the PY-based theory underestimates clustering more relative to the mPY theory as $^{L}/_{D}$ decreases (colloid limit), consistent with earlier observations in the dilute system and general van der Waals arguments[50,61] concerning the influence of attractions on local packing at high densities.[30] $^{L}/_{D} \approx 1$ is a crossover asymmetry ratio below (above) which the needle-induced enhancement of particle contacts is enhanced (very small). This observation is relevant to the large differences between PRISM-mPY and DFT for spinodals boundaries in the $L < D$ colloid regime.

V. Discussion

A new microscopic site−site integral equation approach for needle−sphere suspensions, which includes nonlocal entropic repulsion effects within a thermodynamically self-consistent framework, has been developed. On the basis of model calculations and comparisons with prior theoretical approaches and simulations, our primary conclusions are as follows. (1) PRISM-mPY theory predicts the correct scaling behavior of needle−particle correlations near contact in the dilute needle and dilute particle limits. (2) Predictions of the needle-induced depletion attraction between two particles in a dilute needle solution are in good agreement with exact numerical results and experimental observations. (3) The calculated local colloidal

structure is in good agreement with the very limited simulation data. (4) PRISM-mPY results for the dependence of fluid−fluid spinodal boundaries on L and R are qualitatively different compared to those from previous approaches.[22] The spinodal boundaries collapse as $^{L}/_{D} \rightarrow 0$ in reduced units of c_p/c_p^*, suggesting that large particles (colloids) are not sensitive to the architecture of the small needles. In the large-needle limit ($^{L}/_{D} \rightarrow \infty$), the spinodal boundaries collapse in reduced units of c_pL^2D, consistent with the volume exclusion between needles and particles when a needle is long. These results are in contrast to DFT and SPT, which predict universal behavior for all $^{L}/_{D}$ ratios on the basis of the c_pL^2D variable. Significant differences in the shape of the spinodal curves that are most pronounced at high particle volume fractions are also found.

PRISM calculations (Appendix) of spinodal phase separation for mixtures composed of interacting rods find the same qualitative trends as for ideal needles. This suggests that solvent effects that control the short-ranged needle−needle interaction play a minor role under dilute/semidilute solution conditions. However, other effects such as electrostatic charge are commonly present in polyelectrolyte and biological systems, and the influence of long-range interactions on mixture properties remains to be answered by future simulation and theories. The site−site representation of a rigid rod is a convenient model in which to include noncontact attractive or repulsive interactions between rods and/or polymers and particles.

Finally, by combining the present theory with our prior progress for flexible polymer coils,[28−30] mixtures containing semiflexible chains (e.g., DNA) can be potentially addressed. The introduction of a new length scale, the persistence length, with its potentially highly variable relation to particle diameter is likely to result in new regimes of phase and structural behavior even under ideal or athermal solvent conditions. More generally, the PRISM-mPY ideas can be generalized to a variety of macromolecular architectures, including fractal objects.[63]

Acknowledgment. We are pleased to dedicate this paper to Professor Hans C. Andersen in recognition of his superb contributions to the theoretical understanding of liquids. This material is based upon work supported by the U.S. Department of Energy, Division of Material Sciences under award no. DEFG02-91ER45439 through the Frederick Seitz Materials Research Laboratory at the University of Illinois at Urbana-Champaign. We thank C. Marques and Thierry Savin for sending the exact numerical results data of ref 46, and K.-H. Lin and Arjun Yodh for sending data and preprints of experimental work.

Appendix: Interacting Rods

There have been very few theoretical or simulation studies of mixtures of interacting rods and particles. Here, we briefly examine the fluid−fluid phase behavior of repelling needles and particles at polymer concentrations far below the nematic−isotropic (NI) transition in the absence of particles.

An athermal interacting rod of thickness d has the same self-structure factor as an ideal needle but experiences inter-rod repulsion. We treat this system with the simplified "cutoff thread" model described in depth elsewhere,[64] which has been shown to be adequate for the $L \gg d$ case of interest.[65,66] Because $L \gg d$ and R, the needle mPY result for the nonlocality length λ described in section II is employed. For $c_p > c_p^*$ nondilute rod concentrations, blob scaling ideas are utilized in the semidilute concentration regime[54,66] corresponding to identifying the nonlocality length in the colloid limit with the rod solution mesh size, $\lambda_0 = \xi_\rho$. For hard rods, the cutoff thread model closure is[64]

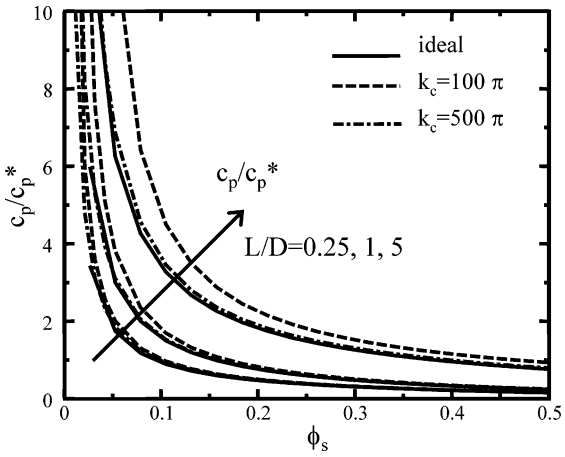

Figure 10. O(c_p) PRISM-mPY spinodal boundaries for athermal rod−particle mixtures with $d_{eff}/L = 0$ (ideal needle), 0.002, and 0.01 for $^{L}/_{D} = 5$, 1, and 0.25, respectively.

$$\hat{C}_{pp}(k) = \begin{cases} C_0 & 0 < k < k_c \\ 0 & k_c < k \end{cases} \tag{A1}$$

where the upper wavevector cutoff $k_c = \pi/d_{eff}$ mimics a rod of thickness d_{eff}. The pure-rod PRISM equation is[64]

$$\hat{h}_{pp}(k) = \frac{\tilde{\omega}_p(k)^2 C_0}{1 - c_p\tilde{\omega}_p(k)C_0} = \tilde{\omega}_p(k)C_0\hat{S}_{pp}(k) \tag{A2}$$

The hard-core site impenetrability condition for the cutoff thread model is $h_{pp}(r \rightarrow 0) = -1$, which when combined with eqs 9 and A2 determines C_0. From eq 8, ξ_ρ may be written as

$$\xi_\rho = \frac{1}{k}\sqrt{\frac{1 - \tilde{\omega}_p(k)}{\tilde{\omega}_p(k)(1 - c_pC_0)}} \overrightarrow{k0} \frac{R_g}{\sqrt{3}}(1 - c_pC_0)^{-1/2} = \frac{R_g}{\sqrt{3}}\frac{1}{\sqrt{1 + 0.39d_{eff}L^2c_p}} \tag{A3}$$

Equation A3 shows the $c_p^{-1/2}$ dependence found by field theory, scaling arguments, experiments, and analytic cutoff PRISM studies.[65] It also suggests that ξ_ρ has a weak c_p dependence on rod concentrations below the NI transition or $c_p^{NI}d_{eff}L^2 \approx 4$. For example, ξ_ρ decreases by approximately 4% ($d_{eff}/L = 0.001$), 25% ($d_{eff}/L = 0.01$), and 66% ($d_{eff}/L = 0.1$) over this concentration range.

At the perturbative O(c_p) level, the spinodals of the athermal needle−particle system are modified only by C_0. From eqs 13 and A1, one obtains

$$c_p^{+} = \left[C_0 + \frac{1}{c_{p,ideal}^{+}}\right] \tag{A4}$$

where $C_0 = 0.39d_{eff}L^2$ and $c_{p,ideal}^{+}$ is the ideal needle concentration at the spinodal. Figure 10 shows typical results. All of the qualitative trends remain the same as those found for the $d_{eff} \equiv 0$ ideal needle model. As expected, the presence of inter-rod repulsion pushes the demixing boundaries to higher values for all size-asymmetry ratios, more so as the particle volume fraction decreases and/or the aspect ratio L/d_{eff} decreases. At low enough ϕ_s, the athermal needle spinodals diverge as previously found for random coil−particle mixtures under athermal solvent

conditions.[28,30] We refrain from plotting the spinodal boundaries to very high values of c_p/c_p^* because the possibility of nematic phase formation has been ignored.

References and Notes

(1) Poon, W.; Pusey, P.; Lekkerkerker, H. N. W. *Phys. World* **1996**, 27.

(2) Poon, W. C. K. *J. Phys.: Condens. Matter* **2002**, *14*, R859.

(3) Russel, W. B.; Saville, D. A.; Schowalter, W. R. *Colloidal Dispersions*; Cambridge University Press: Cambridge, U.K., 1989.

(4) Ilett, S. M.; Orrock, A.; Poon, W. C. K.; Pusey, P. N. *Phys. Rev. E* **1995**, *51*, 1344.

(5) Ramakrishnan, S.; Fuchs, M.; Schweizer, K. S.; Zukoski, C. F. *J. Chem. Phys.* **2002**, *116*, 2201.

(6) Shah, S. A.; Chen, Y. L.; Schweizer, K. S.; Zukoski, C. F. *J. Chem. Phys.* **2003**, *118*, 3350.

(7) Bolhius, P. G.; Louis, A. A.; Hansen, J.-P. *Phys. Rev. Lett.* **2002**, *89*, 128302.

(8) Bolhuis, P. G.; Frenkel, D. *J. Chem. Phys.* **1994**, *101*, 9869.

(9) Bolhius, P. G.; Meijer, E. J.; Louis, A. A. *Phys. Rev. Lett.* **2003**, *90*, 068304.

(10) Louis, A. A.; Bolhius, P. G.; Meijer, E. J.; Hansen, J. P. *J. Chem. Phys.* **2002**, *116*, 10547.

(11) Louis, A. A.; Bolhius, P. G.; Meijer, E. J.; Hansen, J. P. *J. Chem. Phys.* **2002**, *117*, 1893.

(12) Tej, M. K.; Meredith, J. C. *J. Chem. Phys.* **2002**, *117*, 5443.

(13) Gast, A. P.; Hall, C. K.; Russel, W. B. *J. Colloid Interface Sci.* **1983**, *96*, 251.

(14) Asakura, S.; Oosawa, F. *J. Chem. Phys.* **1954**, *22*, 1255.

(15) Asakura, S.; Oosawa, F. *J. Polym. Sci.* **1958**, *33*, 183.

(16) Vrij, A. *J. Chem. Phys.* **1978**, *69*, 1742.

(17) Sear, R. P. *Phys. Rev. Lett.* **2001**, *86*, 4696.

(18) Sear, R. P. *Phys. Rev. E* **2002**, *66*, 051401.

(19) Joanny, J. F.; Leibler, L.; deGennes, P. G. *J. Polym. Sci., Part B: Polym. Phys.* **1979**, *17*, 1073.

(20) Eisenriegler, E. *J. Chem. Phys.* **2000**, *113*, 5091.

(21) Schmidt, M.; Fuchs, M. *J. Chem. Phys.* **2002**, *117*, 6308.

(22) Schmidt, M. *Phys. Rev. E* **2001**, *63*, 050201.

(23) Schmidt, M.; Löwen, H.; Brader, J. M.; Evans, R. *Phys. Rev. Lett.* **2000**, *85*, 1934.

(24) Lekkerkerker, H. N. W.; Poon, W. C. K.; Pusey, P. N.; Stroobants, A.; Warren, P. B. *Europhys. Lett.* **1992**, *20*, 559.

(25) Aarts, D. G. A. L.; Tuinier, R.; Lekkerkerker, H. N. W. *J. Phys.: Condens. Matter* **2002**, *14*, 7551.

(26) Kulkarni, A. M.; Chatterjee, A. P.; Schweizer, K. S.; Zukoski, C. F. *Phys. Rev. Lett.* **1999**, *83*, 4554.

(27) Chatterjee, A. P.; Schweizer, K. S. *J. Chem. Phys.* **1998**, *109*, 10477.

(28) Fuchs, M.; Schweizer, K. S. *Europhys. Lett.* **2000**, *51*, 621.

(29) Fuchs, M.; Schweizer, K. S. *Phys. Rev. E* **2001**, *64*, 021514.

(30) Fuchs, M.; Schweizer, K. S. *J. Phys: Condens. Matter* **2002**, *14*, R239.

(31) Ramakrishnan, S.; Fuchs, M.; Schweizer, K. S.; Zukoski, C. F. *Langmuir* **2002**, *18*, 1082.

(32) Shah, S. A.; Chen, Y. L.; Ramakrishnan, S.; Schweizer, K. S.; Zukoski, C. F. *J. Phys.: Condens. Matter* **2003**, *15*, 4751.

(33) Shah, S. A.; Ramakrishnan, S.; Chen, Y. L.; Schweizer, K. S.; Zukoski, C. F. *Langmuir* **2003**, *19*, 5128.

(34) Adams, M.; Dogic, Z.; Keller, S. L.; Fraden, S. *Nature* **1998**, *393*, 349.

(35) Tracy, M. A.; Garcia, J. L.; Pecora, R. *Macromolecules* **1993**, *26*, 1862.

(36) Tracy, M. A.; Pecora, R. *Macromolecules* **1992**, *25*, 337.

(37) Penfold, J.; Staples, E.; Tucker, I.; Cummins, P. *J. Phys. Chem.* **1996**, *100*, 18133.

(38) Koenderink, G. H.; Vliegenhart, G. A.; Kluijtmans, S. G. J. M.; Blaaderen, A. v.; Philipse, A. P.; Lekkerkerker, H. N. W. *Langmuir* **1999**, *15*, 4693.

(39) Phalakornkul, J. K.; Gast, A. P.; Pecora, R. *J. Chem. Phys.* **2000**, *112*, 6487.

(40) Doi, M.; Edwards, S. F. *Theory of Polymer Dynamics*; Oxford University Press: Oxford, U.K., 1987.

(41) Onsager, L. *Ann. N.Y. Acad. Sci.* **1949**, *51*, 627.

(42) Vliegenthart, G. A.; Lekkerkerker, H. N. W. *J. Chem. Phys.* **1999**, *111*, 4153.

(43) Mao, Y.; Cates, M. E.; Lekkerkerker, H. N. W. *J. Chem. Phys.* **1997**, *106*, 3721.

(44) Chen, Y. L.; Schweizer, K. S. *Langmuir* **2002**, *18*, 7354.

(45) Chen, Y. L.; Schweizer, K. S. *J. Chem. Phys.* **2002**, *117*, 1351.

(46) Yaman, K.; Jeppesen, C.; Marques, C. M. *Europhys. Lett.* **1998**, *42*, 221.

(47) Percus, J. K.; Yevick, G. J. *Phys. Rev.* **1958**, *110*, 1.

(48) Chatterjee, A. P.; Schweizer, K. S. *J. Chem. Phys.* **1998**, *109*, 10464.

(49) Chandler, D.; Andersen, H. C. *J. Chem. Phys.* **1972**, *57*, 1930.

(50) Chandler, D. Equilibrium Theory of Polyatomic Fluids. In *Studies in Statistical Mechanics*; North-Holland: Amsterdam, 1982; Vol. 8; p 274.

(51) Chen, Y. L.; Schweizer, K. S.; Fuchs, M. *J. Chem. Phys.* **2003**, *118*, 3880.

(52) Lebowitz, J. L.; Rowlingson, J. S. *J. Chem. Phys.* **1964**, *41*, 133.

(53) Curtin, W. A.; Ashcroft, N. W. *Phys. Rev. A* **1985**, *32*, 2909.

(54) deGennes, P. G. *Scaling Concepts in Polymer Physics*; Cornell University Press: Ithaca, NY, 1979.

(55) Schweizer, K. S.; Curro, J. G. *Adv. Chem. Phys.* **1997**, *98*, 1, and refs cited therein.

(56) Schweizer, K. S.; Curro, J. G. *Adv. Polym. Sci.* **1994**, *116*, 319.

(57) Reiss, H.; Frish, H. L.; Lebowitz, J. L. *J. Chem. Phys.* **1959**, *31*, 369.

(58) Lin, K.-H.; Crocker, J. C.; Zeri, A. C.; Yodh, A. G. *Phys. Rev. Lett.* **2001**, *87*, 088301.

(59) Lau, A. W. C.; Lin, K.-H.; Yodh, A. G. *Phys. Rev. E* **2002**, *66*, 020401.

(60) Carnahan, N. F.; Starling, K. E. *J. Chem. Phys.* **1970**, *53*, 600.

(61) Hansen, J. P.; McDonald, I. R. *Theory of Simple Liquids*, 2nd ed.; Academic Press: London, 1986.

(62) Kirkwood, J. G.; Buff, F. P. *J. Chem. Phys.* **1951**, *19*, 774.

(63) Fuchs, M.; Schweizer, K. S. *J. Chem. Phys.* **1997**, *106*, 347.

(64) Pickett, G. T.; Schweizer, K. S. *J. Chem. Phys.* **2000**, *112*, 4869.

(65) Wang, X.; Chatterjee, A. P. *J. Chem. Phys.* **2003**, *119*, 12629.

(66) Chatterjee, A. P. Unpublished results.